

MOHAMED AFQIR^{1*}, STEVAN STOJADINOVIC², MOHAMED ELAATMANI¹,
 ABDELOUAHAD ZEGZOUTI¹, NABIHA TAHIRI¹, MOHAMED DAOUUD¹

HYDROTHERMAL SYNTHESIS, IMPEDANCE AND OPTICAL PROPERTIES OF Tm-DOPED SrBi₂Nb₂O₉ CERAMICS

In this study, Strontium Bismuth Niobate (SrBi_{2-x}Tm_xNb₂O₉ with $0 \leq x \leq 0.1$) doped by Tm was synthesized using by the hydrothermal method. The microstructure and electrical properties were mainly investigated. XRD analysis showed a single-phase orthorhombic structure for Tm-doped SrBi₂Nb₂O₉ samples. The crystallite size is anisotropic and the strain is apparently independent of Tm amount. Dielectric properties for doped SrBi₂Nb₂O₉ with Tm³⁺ ion have the same trend discussed for the pure sample. FTIR results showed that NbO₆ octahedral is formed, on one hand, and on the other hand, it shows that spectra for doped and undoped samples are nearly the same. The Cross-section of ceramics showed the plate-like morphology, also the distribution of the pore in ceramics are observed for all samples. Tm dopants produce only minor changes in the impedance parameter values at room temperature. The luminescent (PL) properties of Tm-doped SrBi₂Nb₂O₉ ceramic powders were investigated. The optimum Tm³⁺ concentration for the maximum PL intensity was found to be at $x = 0.075$.

Keywords: hydrothermal; microstructure; impedance; luminescent

1. Introduction

SrBi₂Nb₂O₉ materials belong Bismuth layer-structured ferroelectrics (BLSFs) family. Because of their excellent fatigue endurance, fast switching speed, good polarization retention, relatively high Curie temperature, low aging rate, and low operating voltage, BLSFs are commercially applicable as ferroelectric non-volatile random-access memory (FRAM) storage devices [1]. In our previous work, We have explained the effect of rare-earth ions (RE³⁺) substitution for Bi³⁺ on various properties of SrBi_{2-x}RE_xNb₂O₉ ($0 \leq x \leq 0.5$) ceramics prepared by solid-state method. Substitution of RE³⁺ for Bi³⁺ in SrBi₂Nb₂O₉ induced a shift in the Curie temperature to lower values along with an introduction of relaxor behavior when the amount of substitution being about 30 mol %. Meanwhile, oxygen vacancies responsible for the dielectric losses in SrBi₂Nb₂O₉ ceramics, which are formed as a result of Bi³⁺ volatilization during high-temperature processing greater than 1100°C, could be stabilized by the introduction of rare-earth ions in the SrBi₂Nb₂O₉ lattice structure. SrBi₂Nb₂O₉ structure is composed of (Bi₂O₂)²⁺ layers and (SrNb₂O₉)²⁻ perovskite-like blocks. In this mate-

rial, the intrinsic oxygen vacancies of fluorite-like structure, (Bi₂O₂)²⁺, have been confirmed [2]. In addition, doping with a small amount of certain rare-earth could reduce the amount of oxygen vacancies.

Various methods like the conventional solid-state method, co-precipitation, hydrothermal method, were used to prepare SrBi₂Nb₂O₉ compounds. Instead of the solid-state method, chemical routes (*i.e.* co-precipitation) provide a lower formation temperature (<1000°C). The main advantage of the wet-chemistry routes, it plays the part of the solvent, thus permits the production of high-purity and homogeneous ceramic powder.

The luminescence properties of SrBi₂Nb₂O₉ materials doped with rare-earth ions have not been widely studied. Under 451 nm light excitation, Ho-doped SrBi₂Nb₂O₉ exhibited a strong green emission centered at 545 nm due to the intra f-f transition from the excited to the ground state of Ho³⁺ ions and the concentration quenching effect was observed when reaching 0.4 mol% [3]. In Sr_{0.7}Er_xBi_{2.2-x}Nb₂O₉ ($x = 0.0, 0.4, 0.6, 0.8, 1$) Opto-electro materials, Er³⁺ ions showed four intense emission bands peaking around 424 (violet), 444 (violet), 464 (Blue), 478 (Blue) [4]. Photoluminescence properties of Pr³⁺-doped

¹ UNIVERSITÉ CADI AYYAD, FACULTÉ DES SCIENCES SEMLALIA, LABORATOIRE DES SCIENCES DES MATÉRIAUX ET OPTIMISATION DES PROCÉDÉS, MARRAKECH, MOROCCO

² UNIVERSITY OF BELGRADE, FACULTY OF PHYSICS, STUDENTSKITRG 12-16, BELGRADE, SERBIA

* Corresponding author: mohamed.afqir@yahoo.fr



SrBi₂Nb₂O₉ compounds showed red emission and the optimal emission intensity was obtained when Pr³⁺ concentration reach 0.005 mol under the 250-350 nm ultraviolet excitations [5]. SrBi₂Nb₂O₉ doped by Eu³⁺ showed bright photoluminescence upon blue light excitation of the 400-500 nm. Upon the excitation of 465 nm light, the materials have two intense emission bands peaking around 593 nm (yellow) and 616 nm (red). Meanwhile, the strongest emission was observed for 4 mol % [6].

It should be noted that the materials discussed here, have not been synthesized yet by the hydrothermal process. The aim of this study is the synthesis and room temperature characterization of low doping-Aurivillius phases SrBi_{2-x}Tm_xNb₂O₉ (0 ≤ x ≤ 0.1) prepared by hydrothermal process.

2. Experimental

Appropriate amounts of Bi₂O₂ (Rectapur, 99%), Nb₂O₅ (Acros Organics, 99.5%), Tm₂O₅, and SrCO₃ (Aldrich, 99.9%) were mixed and homogenized in KOH (10 M) solution. They were poured into an autoclave followed by 20 vol% distilled water and heated at 200°C. After 48 h at 200°C, the samples were filtered and dried at 100°C. The powders were pressed uniaxially to 1 t/cm² to form a pellet (thickness: 1mm and diameter: 6 mm). The pellets were sintered, at the air, at 1200°C for one hour. The samples were examined through X-ray diffraction of Rigaku monochromatized CuK_α radiation (λ = 1.54 Å). Scan step: 0.02 deg, scan speed: 5 deg/min, and scan Resolution: 0.002 were parameters that used for XRD measurement. Fourier-transform infrared spectroscopy recorded on KBr pellets Bruker Vertex 70 and their microstructure were performed with a scanning electron microscopy EDAX AMETEK. Dielectric measurements were performed using SMART Impedance from 1 Hz to 1 MHz. Photoluminescence measurements were obtained utilizing a Horiba Jobin Yvon Fluorolog FL3-22 spectrofluorometer, with a 450 W xenon lamp as an excitation light source.

3. Results and discussion

Figure 1 shows the XRD patterns of Tm-doped SrBi₂Nb₂O₉ ceramic powders. All peaks corresponding to the SrBi₂Nb₂O₉ (01-086-1190) are detected in prepared samples. (115) reflection is an isolated well-defined peak which is characteristic for layers structure Aurivillius phases. Table 1 shows the unit cell parameters obtained by UnitCell program in the solid solution, refined in the orthorhombic system, using wavelength 1.540593 Å. Solid solutions do not follow Vegard's law which the lattice parameter varies linearly [7]. The expansion of the cell is smoothly changed with the replacement of the larger Bi³⁺ ion (1.02 Å) with the smaller Tm³⁺ ion (0.869 Å) [8], may the Tm amount does not sufficient to bring significant affecting on the parameter values. A Williamson-Hall method permits to deduce crystallite size with strain, taking into account instrumental broadening [9].

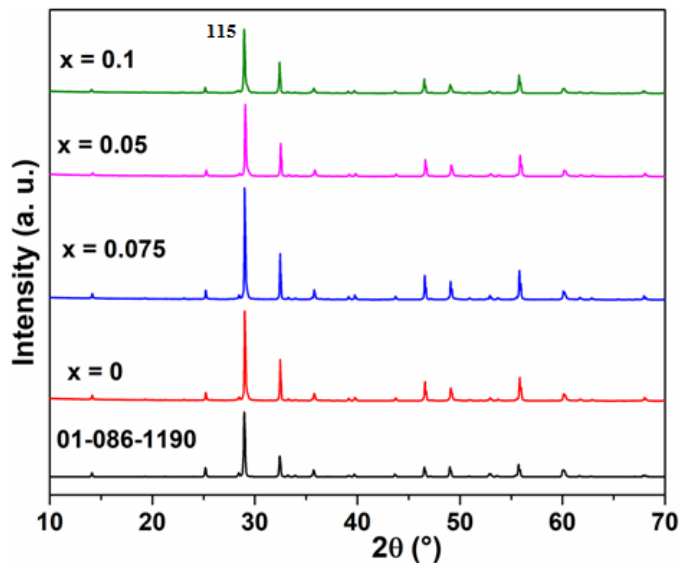


Fig. 1. XRD spectra of Tm-doped SrBi₂Nb₂O₉ ceramic powders

TABLE 1

XRD cell parameters of Tm-doped SrBi₂Nb₂O₉ ceramic powders

Parameter	x = 0	x = 0.05	x = 0.075	x = 0.1
a (Å)	5.511	5.501	5.507	5.499
b (Å)	5.516	5.517	5.503	5.500
c (Å)	25.118	25.079	25.116	25.064
Cell vol (Å ³)	763.553	761.098	761.168	758.046

Estimation of crystallite size (D) by Williamson-Hall-isotropic strain model is given by the following equation:

$$\beta \cos \theta = \frac{\lambda}{D} + 4\varepsilon \sin \theta$$

In order to understand the contributions of lattice strain and crystalline size to the XRD peaks a Williamson-Hall can be shown with the average values using the High Score Analytical program. Figure 2 shows crystallite size and strain (ε) for SrBi₂Nb₂O₉ ceramic powders data. A small contribution of microstrain, with no evident dependence of Tm amount, compared to that obtained at (0010) reflection which shows the highest value of crystallite size. The contribution of microstrain is inversely proportional to crystallite size. When The elastic deformation is not uniform in all crystallographic directions, uneven distribution of crystallite size with no evident dependence with Tm concentration and (hkl) reflection. The average crystallite size is small for x = 0.1 compared to other dopants.

Figure 3 shows the FTIR spectra of Tm-doped SrBi₂Nb₂O₉ ceramic powders. Spectra are plotted as a function of transmittance (arbitrary unit: a. u.). All samples contain absorbed H₂O (3400 cm⁻¹) and two principal absorption bands at 590 and 483 cm⁻¹ corresponding to the stretching vibration oxygen-niobium of NbO₆ octahedral [10]. These two bands are a characteristic SrBi₂Nb₂O₉ structure. Therefore, the position of the main bands does not change with doping.

SEM images are shown in Figure 4. SEM photographs of fracture surface show plate-like crystal morphology. The

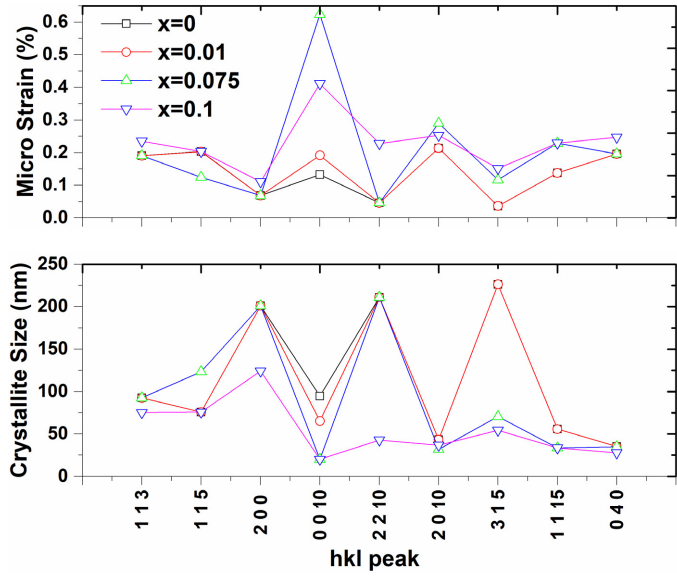


Fig. 2. Crystallite size and strain for SrBi₂Nb₂O₉ ceramic powders

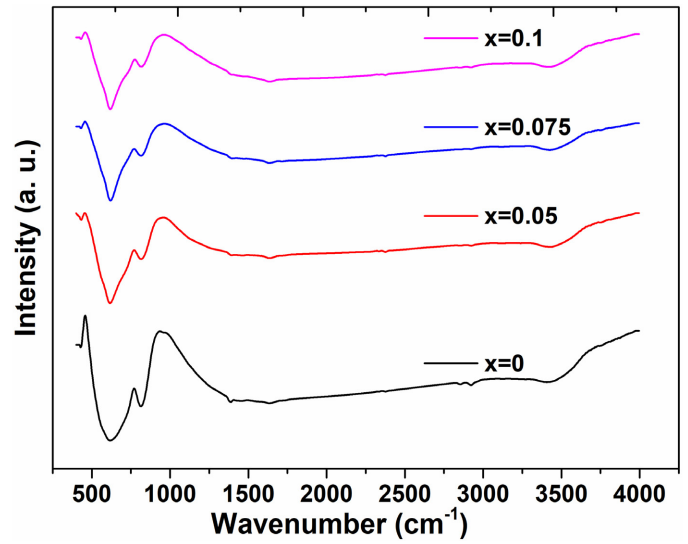


Fig. 3. FTIR spectra of Tm-doped SrBi₂Nb₂O₉ ceramic powders

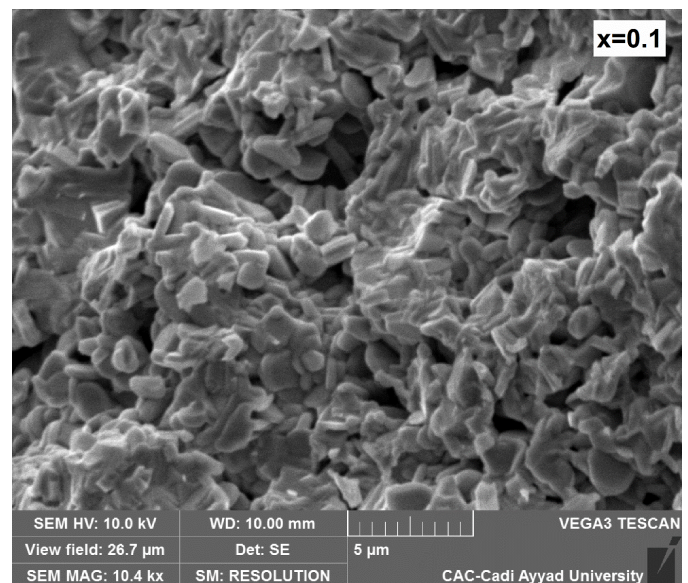
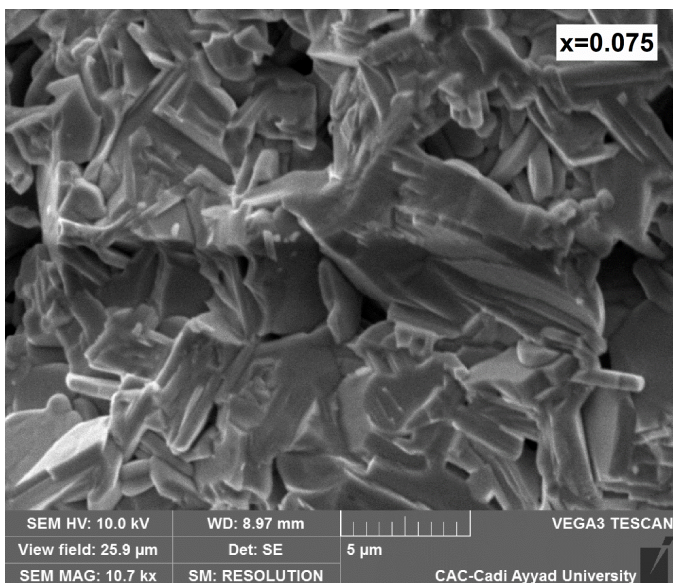
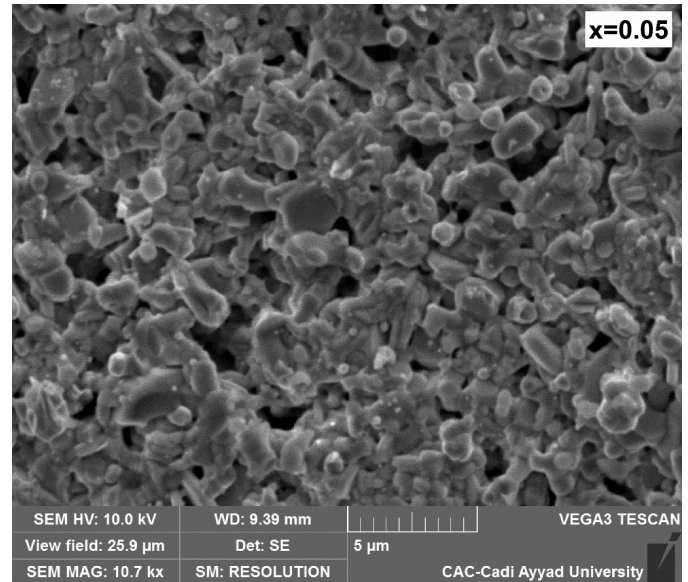
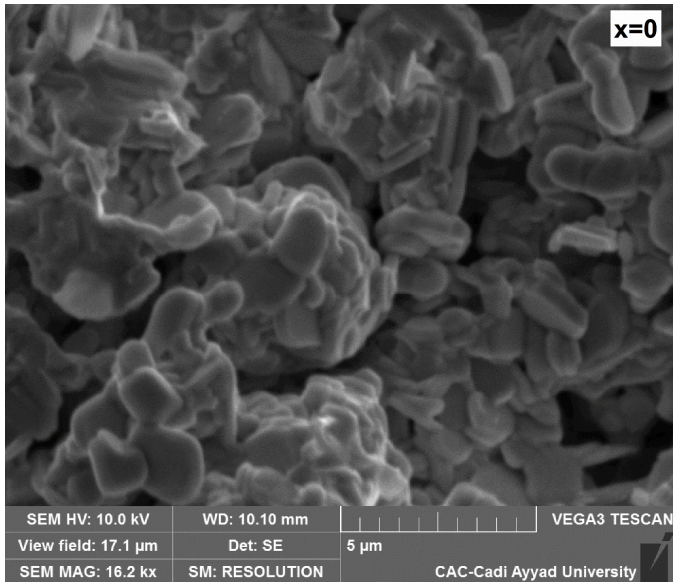


Fig. 4. SEM images of Tm-doped SrBi₂Nb₂O₉ ceramics

average grain size varies between 1 μm and 400 nm. Except for $x = 0.075$, the boundaries of the plate-like structure are not very sharp. The sample $x = 0.075$ shows a dense morphology with a larger average grain size compared to undoped and the other doped ceramics. The grains size that comes from SEM is different than crystallite size obtained from the Williamson Hall method. This difference can be explained by the fact that a grain is made up of several crystallites.

The temperature dependence of the dielectric constants and dielectric loss at room temperature of Tm-doped $\text{SrBi}_2\text{Nb}_2\text{O}_9$ ceramics are shown in Figure 5. The dielectric constants decrease firstly and then remain constant with increasing frequency around 117 when measured at 1 MHz. The dielectric constant is about 235, 180, 344, 277 for $x = 0.1, 0.05, 0.075,$ and 0.1 respectively when measured at 10 kHz. The dielectric loss decrease with increasing frequency. however, the doping has a small effect on dielectric loss at low frequency inferior than 10 kHz. Meanwhile, at the high frequency, it's found to be around 0.09 when measured at 1 MHz. The sharp drop of dielectric constants at low frequency is mainly due to space charges [11]. The evolution of these two dielectric parameters seems to be independent of doping which could be attributed to the grain size and the density of the ceramics [12].

Figure 6 shows the Nyquist and Bode plots of impedance at room temperature of Tm-doped $\text{SrBi}_2\text{Nb}_2\text{O}_9$ ceramics. Figure

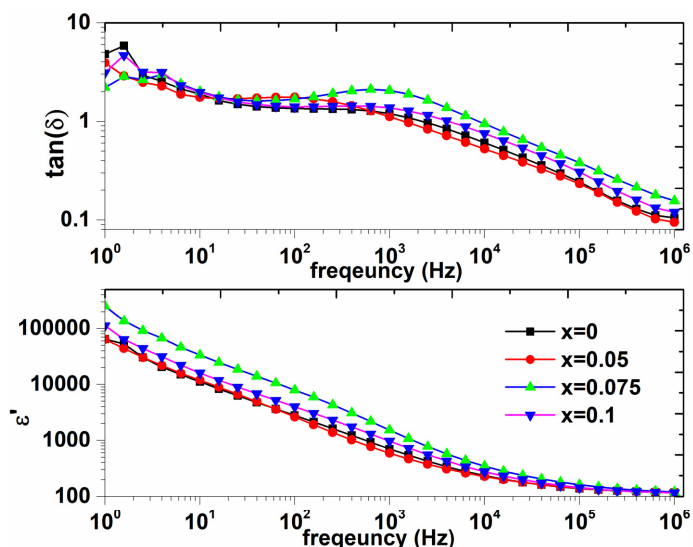


Fig. 5. Frequency dependence of the dielectric constants and dielectric loss at room temperature of Tm-doped $\text{SrBi}_2\text{Nb}_2\text{O}_9$ ceramics

res present impedance magnitude ($|Z|$) and impedance phase degrees as a function of frequency. The impedance magnitude of all samples decreases with the increasing Tm amount, except $x = 0.01$ which the impedance magnitude has put up smoothly compared to other dopants. However, at a higher frequency

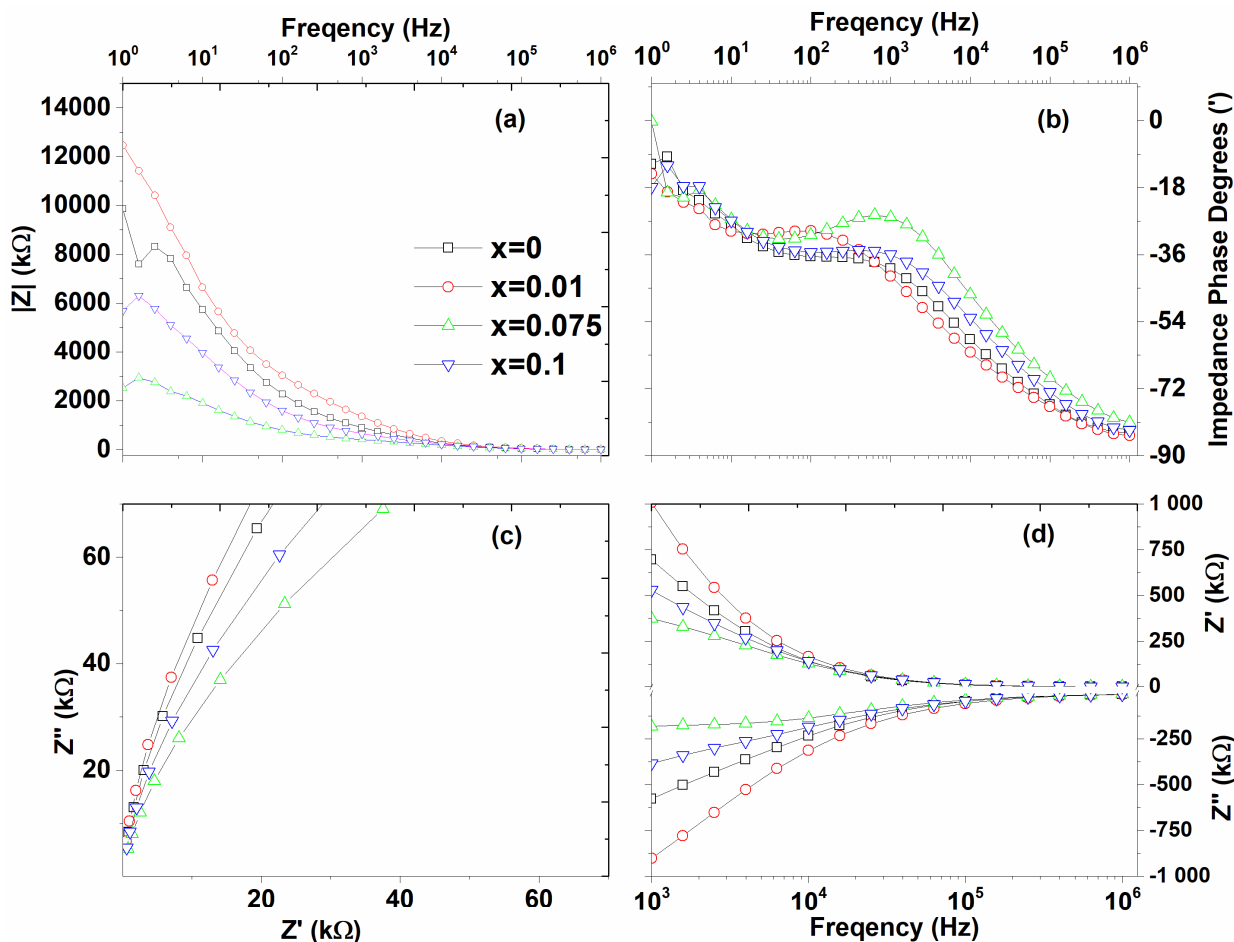


Fig. 6. Bode and Nyquist plots at room temperature of Tm-doped BaTiO_3 ceramics

greater than 100 kHz, the magnitude remains constant around 46 k Ω for all samples.

The frequency dependence of impedance phase degrees follows the same trend with one relaxation process. This dissipation peak appeared at frequency 1 kHz, does not shift with increasing Tm amount. Meanwhile, the low-frequency behavior of the phase angle ($\sim\pi/7$) suggests the existence of a transport process through the ceramics that is best described as the physical dimensions and materials of the transmission line [13]. This means that the current leads the voltage by 87 degrees and the reactance could be capacitive.

The real (Z') versus imaginary (Z'') parts of the complex impedance involves an arc of a circle as shown in Figure 6c. A single arc indicating that the electrical process occurring in these materials has a single relaxation due to the contribution of the grain and grain boundaries. The compositions $x = 0.075$ and $x = 0.1$ have the complex impedance radius smaller than the other ones.

Frequency dependence of imaginary (Z'') and real (Z') parts of impedance at different Tm concentration, reveals that when the real part decreases, the imaginary part increases with increasing frequency until 10 kHz, then high-frequency data tend to become bunched together around 205 k Ω and 8531 k Ω for Z'' and Z' respectively.

Figure 7a shows the emission photoluminescence spectra of Tm-doped SrBi₂Nb₂O₉ ceramic powders excited at 375 nm. The Tm-doped SrBi₂Nb₂O₉ compounds show a strong blue luminescence at 440 nm, consists of the f-f transition lines within the Tm³⁺ 4f¹² electron configuration (¹D₂ \rightarrow ³F₄ transition) [14,15].

Figure 7b shows the excitation photoluminescence spectra monitored at 440 nm. The Bi³⁺ ion with a 6s² electronic configuration shows strong optical absorption in the near-ultraviolet

region (270 nm) due to the s²-sp transition [5]. The narrow line at about 375 nm can be ascribed to the characteristic f-f transition (³H₆ \rightarrow ¹D₂) of Tm³⁺ within its 4f¹² configuration [14].

The optimum Tm³⁺ concentration for the maximum photoluminescence intensity was found to be at $x = 0.075$. Up to $x = 0.1$, the photoluminescence intensity decreased due to the quenching. Thus, when the Tm³⁺ concentration increases, the distance between the Tm³⁺ ions decreases, involving non-radioactive energy transfers between Tm³⁺ ions [16].

It has been assumed that the process of synthesis contributes to the variation of intensity, widening, and a shift of XRD peaks. SrBi₂Nb₂O₉ sample synthesized through molten salt route evidenced the presence of plate-like grains. However, the same sample exhibits predominantly polygonal-shaped grains when synthesized through the oxalate co-precipitation route [17]. The hydrothermal route is the least expensive regarding co-precipitation or solid-state methods. The dielectric and electrical properties were controlled by the physical dimensions of the grain. The preparation of ceramics by the solid-state method offers a high dielectric constant compared to the hydrothermal process [18].

4. Conclusion

A hydrothermal method was used to prepare Thulium doped strontium bismuth niobate ceramics. The synthesized samples were characterized by X-ray powder diffraction (XRD), Infrared spectroscopy (FTIR). $X = 0.075$ exhibits densest ceramic. Based on results obtained from XRD and SEM, grains contain several crystallites. The Tm element was explored in this study as an inhibitor of oxygen vacancy. The Nyquist and Bode of impedance

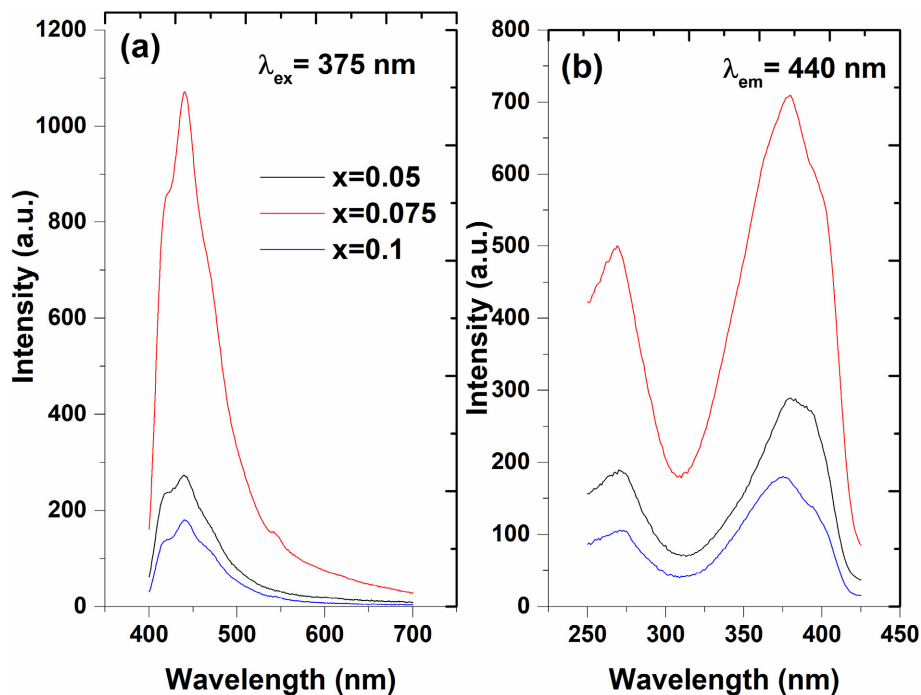


Fig. 7. Emission and excitation photoluminescence spectra of Tm-doped SrBi₂Nb₂O₉ ceramic powders

measured at room temperature suggest that the materials have one single relaxation. The observed differences have been attributed to the presence of Tm in the strontium bismuth niobate ceramics. At high Tm³⁺ concentration 0.1 mol%, the Photoluminescence intensity decreased due to concentration quenching.

REFERENCES

- [1] B.H. Park, B.S. Kang, S.D. Bu, T.W. Noh, J. Lee, W. Jo, *Nature* **401**, 682 (1999).
- [2] A.C. Palanduz, D.M. Smyth, *J. Electroceramics* **11**, 191 (2003).
- [3] L. Yu, J. Hao, Z. Xu, W. Li, R. Chu, *Phys. Status Solidi* **214**, 1700276 (2017).
- [4] A. Tomar, S. Kasana, R.P. Tandon, *AIP Conf. Proc.* **2006**, 030032 (2018).
- [5] H. Zou, Y. Yu, J. Li, Q. Cao, X. Wang, J. Hou, *Mater. Res. Bull.* **69**, 112 (2015).
- [6] L. Yu, J. Hao, Z. Xu, W. Li, R. Chu, G. Li, *Ceram. Int.* **42**, 14849-14854 (2016).
- [7] M.J. Lambregts, S. Frank, *Talanta* **62**, 627 (2004).
- [8] R.D. Shannon, C.T. Prewitt, *Acta Crystallogr. Sect. B Struct. Crystallogr. Cryst. Chem.* **B25**, 925 (1969).
- [9] J.I. Langford, D. Louër, *Appl. Crystallogr.* **33**, 964 (200AD).
- [10] M. Verma, A. Tanwar, K. Sreenivas, V. Gupta, *Ferroelectrics* **404**, 233 (2010).
- [11] F. Rehman, L. Wang, H.-B. Jin, A. Bukhtiar, R. Zhang, Y. Zhao, J.-B. Li, *J. Am. Ceram. Soc.* **100**, 602 (2017).
- [12] Chitra, K.C. Singh, *Ferroelectrics* **518**, (2017).
- [13] E. Barsoukov, J.R. Macdonald, John Wiley Sons, Inc (2005).
- [14] Y. Lu, X. Tang, L. Yan, K. Li, X. Liu, M. Shang, C. Li, J. Lin, *J. Phys. Chem. C* **117**, 21972-21980 (2013).
- [15] G. Li, C. Li, C. Zhang, Z. Cheng, Z. Quan, J. Lin, *J. Mater. Chem.* **19**, 8936 (2009).
- [16] M. Ilhan, R. Samur, H. Demirer, *Metalurgija* **54**, 407 (2015).
- [17] M. Afqir, A. Tachafine, D. Fasquelle, M. Elaammani, J.C. Carru, A. Zegzouti, O. Abdelhamid, M. Daoud, *Sci. Sinter.* **51**, 353 (2019).
- [18] H. Menasra, K. Bounab, Z. Necira, A. Meklid, A. Boutarfaia, *Int. J. Thin Film Sci. Technol.* **9**, 181 (2020).